Falsini *et al. Journal of the European Optical Society-Rapid Publications* (2021) 17:8
https://doi.org/10.1186/s41476-021-00153-y

Journal of the European Optical Society-Rapid Publications

RESEARCH Open Access

A new route for caesium lead halide perovskite deposition

Naomi Falsini[1,2*], Andrea Ristori[2], Francesco Biccari[1,2], Nicola Calisi[3,4], Giammarco Roini[5], Paolo Scardi[6], Stefano Caporali[3,4] and Anna Vinattieri[1,2,7]

Abstract

Inorganic metal halide perovskites are relevant semiconductors for optoelectronic devices. The successful deposition of thin films of $CsPbBr_3$ and $CsPbCl_3$ has recently been obtained by Radio-Frequency magnetron sputtering. In this work we compare the morphological, structural and optical characteristics of the two materials obtained with this deposition technique. A detailed photoluminescence (PL) spectroscopy study of the as-grown samples was conducted at the macro and micro scale in a wide temperature range (10-300 K) to fully characterize the PL on sample areas of square centimeters, to assess the origin of the inhomogeneous broadening and to quantify the PL quantum yield quenching. Our results prove that this technique allows for the realization of high quality nanometric films with controlled thickness of relevance for optoelectronic applications.

Keywords: Perovskites, Time resolved spectroscopy, Photoluminescence, Sputtering, Films

Introduction

Inorganic metal halide perovskites (IMHP) are an emerging class of semiconductors for photonics, photovoltaics and optoelectronics [1–4]. The interest to investigate such kind of perovskites comes from their promising properties: the highly-efficient radiative recombination, being direct bandgap materials; the tunability of light emission, by varying the material composition to cover the entire visible spectral range [5–7]; the robustness towards defects [8–10]; the high carrier mobility; the low-cost and easiness of synthesis and deposition, unlike other semiconductors (Si, GaAs, GaN, etc.) commonly used for applications of interest. The latter is a crucial aspect; indeed the processes typically required for the fabrication of solid-state light emitters and solar cells are expensive, running counter to the demand of the market for low-cost devices. Moreover, the material morphology, which determines the final features and quality of a device based on IMHP, can be easily controlled, from bulk to ordered nano/micro-structures and polycrystalline thin films, by choosing the proper growth protocol [11, 12]. When compared to hybrid halide perovskites, IMHP exhibit significantly improved long-term stability, keeping the same excellent optoelectronic properties [13, 14]. In the last decades, hybrid perovskites (in particular $CH_3NH_3PbI_3$) proved to be particularly interesting for applications in energy harvesting, but they suffer from poor long-term stability (few thousands of hours [15]) due to the rapid degradation of their organic component. Therefore, significant efforts of the research have been recently directed to improve the stability of hybrid perovskites and to develop high quality fully inorganic perovskites. In particular, caesium lead halide perovskites ($CsPbX_3$ X=Cl, Br, I) are excellent candidates for the realization of high-performance light emitters that cover the UV-visible spectral range. $CsPbBr_3$, having a bandgap at 2.3 eV, could help in overcoming the green gap problem of nitrides for realizing green LEDs [16], whereas $CsPbCl_3$, with a bandgap around 3 eV, shows an efficient blue emission useful for white light generation, when coupled with a converting phosphor. White light generation can also be

*Correspondence: naomi.falsini@unifi.it
[1]Department of Physics and Astronomy, University of Florence, via G. Sansone 1, I-50019 Sesto Fiorentino, Italy
[2]European Laboratory for Non-Linear Spectroscopy - LENS, via Nello Carrara 1, I-50019 Sesto Fiorentino, Italy
Full list of author information is available at the end of the article

obtained by multilayer structures of $CsPbCl_3$, $CsPbBr_3$ and $CsPbI_3$.

However, one of the main problems that limits the scalability of the material for innovative perovskite-based devices comes from the lack of sample homogeneity over large areas. Solution-based techniques, which represent the most common route used for the deposition of perovskite thin films, do not guarantee the control of the homogeneity over an area of several square centimeters, being therefore unsuitable for industrial production of devices. Moreover, these techniques cannot be used for the realization of $CsPbCl_3$ films because of the lack of proper solvents for its deposition.

We have recently demonstrated the first successful deposition of polycrystalline thin films of fully inorganic perovskites ($CsPbBr_3$ and $CsPbCl_3$) by Radio-Frequency (RF) magnetron sputtering [17, 18]. Such physical vapor deposition technique [19–21] is widely used for realization of thin films for industrial applications, such as optical coatings, thin films resistors, layers for catalysis, etc. In recent years it was used for the deposition of hybrid perovskites [22]; this technique offers numerous advantages, allowing for film deposition on different kind of substrates and multilayers deposition. By means of such technique we succeeded in obtaining films with a good degree of compactness and homogeneity concerning the material optical properties at a micro-scale and macro-scale level.

The focus of this work is the comparison between thin films of $CsPbCl_3$ and $CsPbBr_3$ grown by RF magnetron sputtering: a particular attention is devoted to the analysis of the materials optical properties.

Methods

Several films of $CsPbCl_3$ and $CsPbBr_3$ with thickness in the range from 70 to 140 nm were deposited by RF magnetron sputtering onto properly cleaned soda lime glass (SLG) substrates [17, 18].

$CsPbX_3$ powder was obtained through a mechanochemical procedure described in literature [23]. It consists in the grinding of the two precursor salts (CsX and PbX_2) in equal molar ratio in a mixer mill (Retsch model MM400) [17, 18]. The sputtering target (5 cm diameter disk) was realized by pressing the perovskite powder by means of a pneumatic press (11.5 MPa working pressure) for 24 h at 150°C. The magnetron sputtering equipment is a Korvus HEX (Korvus Technology Ltd.) equipped with an RF source working at 13.56 MHz. The deposition was performed at room temperature with an RF power of 20 W and argon gas flow of 20 sccm. In these conditions, the dynamic working pressure was $2 \cdot 10^{-6}$ atm and the deposition rate resulted to be in the range from 5 to $7 \cdot 10^{-2}$ nm s^{-1}. The film thickness was monitored during the deposition by using a quartz crystal nanobalance until it reached the desired value. During this time, the sample holder was kept rotating to assure thickness homogeneity.

Optical characterization was performed by photoluminescence (PL) spectroscopy in a wide temperature range (from 10 to 300 K) with different kind of experiments conducted at the macro-scale (excited area $\sim 10^4$ μm^2) and micro-scale (excited area ~ 1 μm^2). Continuous wave (CW) PL experiments were performed by standard setup exciting the PL with different laser sources in the range 266-400 nm. Time-resolved PL spectra were acquired by a streak camera after excitation of the sample at ~ 365 nm with a frequency doubled 1.2 ps mode-locked Ti:Sapphire laser with a time resolution of ~ 5 ps. In both kind of experiments the sample was excited in a quasi backscattering geometry and the PL spectral resolution was 1 meV.

The transmittance measurements were performed by means of a white Xenon lamp; the macro-PL and transmittance spectra were acquired at the same time on the same sample spot.

For micro-photoluminescence (micro-PL) measurements the samples were kept in a low-vibration Janis ST-500 cryostat, which in turn was mounted on a Physik Instrumente x-y translation stage for scanning the sample surface. The PL was collected by a home-made confocal microscope setup equipped with a Mitutoyo 100x objective (378-806-3, NA = 0.7) or a Mitutoyo 50x objective (378-818-4, NA = 0.42). The micro-PL signal was spectrally dispersed and detected using an Acton SP2330i spectrograph, mounting a 1200 gr/mm grating blazed at 300 nm or at 750 nm, and a Si CCD Acton Pixis 100F. The spatial resolution of the system is about 500 nm (1 μm) with the 100x (50x) objective, while the spectral resolution is about 250 μeV. The excitation source was provided by a mode-locked Ti:Sapphire tunable laser (Spectra Physics Tsunami, 700-900 nm spectral range, 200 fs pulse duration, 12.2 ns pulse period) frequency doubled by a BBO crystal and pumped by a frequency doubled CW Nd-YAG laser.

Results and discussion

In this paper we present results of 70 nm thick $CsPbBr_3$ and $CsPbCl_3$ films grown on glass by RF magnetron sputtering [17, 18]: similar results are found for 140 nm thick samples.

Morphological and structural characterization

The as-grown samples appear to be quite compact at a micro-scale level as from the SEM micrographs reported in Fig. 1a for $CsPbBr_3$ and in Fig. 1c for $CsPbCl_3$. From these morphological results, it appears that the samples are characterized by a continuous network of several tens of nanometer size crystals with a random distribution of bigger crystals with typical micrometer/sub-micrometer size, unlike typical spin-coated films where an ensemble of

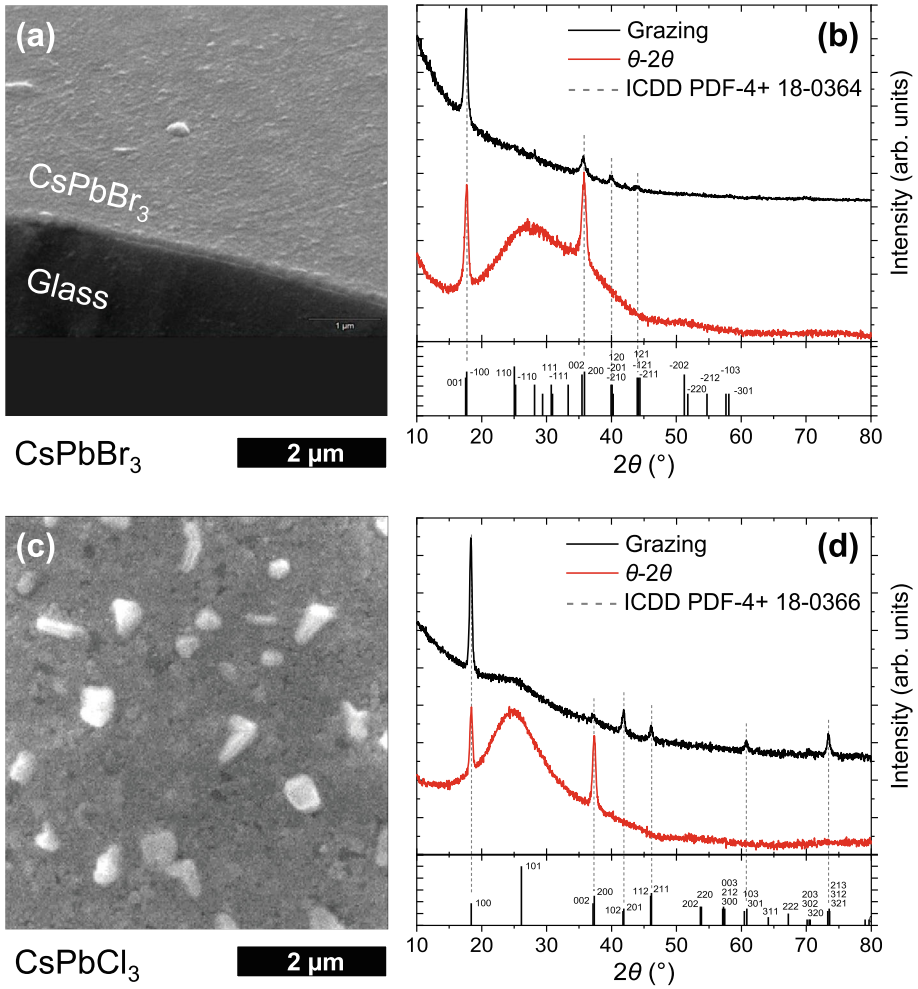

Fig. 1 SEM micrograph (**a**) and XRD spectra (**b**) of a $CsPbBr_3$ sample; SEM micrograph (**c**) and XRD spectra (**d**) of a $CsPbCl_3$ sample

separate crystals is commonly found [24]. Scanning near-field optical microscopy (SNOM) topography map (not shown), acquired for the 70 nm thick $CsPbBr_3$ sample, indicates that the mean film thickness is about 72 nm and the surface roughness is slightly less than 20 nm over an area of several tens of square micrometers.

The room temperature XRD spectra for both samples (grazing incidence in black and θ-2θ in red), shown in Fig. 1b and in Fig. 1d, clearly indicate the presence of the correct crystalline phase for $CsPbBr_3$ (ICDD PDF-4+ 18-0364) and $CsPbCl_3$ (ICDD PDF-4+ 18-0366), orthorhombic (group 62) [25] and tetragonal (group 99) [26] crystalline phase respectively. The broad band in θ-2θ configuration originates from the glass substrate. In θ-2θ pattern two strong (h00) lines, observed in both samples, suggest the presence of a significant amount of textured grains along the [001] directions perpendicular to the substrate, confirmed by the SEM micrographs of Fig. 1. In the grazing incidence condition, instead, the larger crystals contribute only to the (100) line and the presence of small peaks suggests that the nanocrystalline network lacks of orientation.

Optical characterization

In Fig. 2 optical images and room temperature micro-PL maps, acquired in the same sample area, are shown for $CsPbBr_3$ and $CsPbCl_3$ along with typical spectra extracted from the PL maps. For both $CsPbBr_3$ and $CsPbCl_3$ the intensity of the micro-PL, shown in Fig. 2b, is uniform except for the presence of hot spots: the average PL value and the standard deviation are $(9\pm4)\cdot10^3$ arb. units for $CsPbBr_3$ and $(1.2\pm0.5)\cdot10^3$ arb. units for $CsPbCl_3$. The average value and the standard deviation of the PL peak energy (Fig. 2c) are (2.372 ± 0.007) eV for $CsPbBr_3$ and (3.007 ± 0.010) eV for $CsPbCl_3$, indicative of a very good degree of homogeneity of the spectral characteristics.

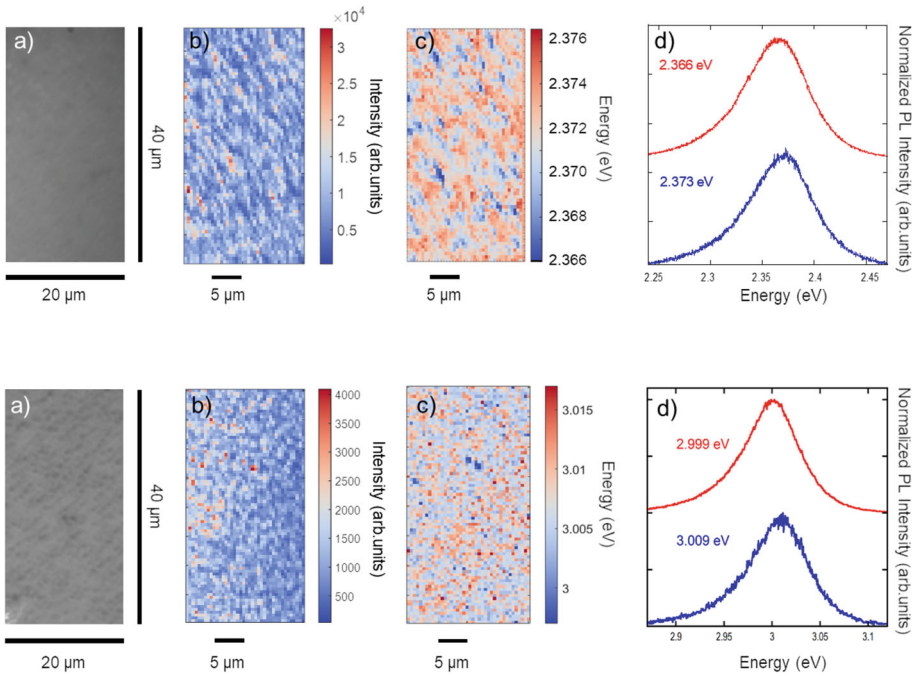

Fig. 2 Micro-PL measurements at room temperature of (upper panel) $CsPbBr_3$ and (lower panel) $CsPbCl_3$ samples deposited on glass: **a**) Optical image of the sample acquired in a 20 × 40 μm^2 area; **b**) PL intensity variations in the same sample area; **c**) Energy of the PL peak in the same sample area; **d**) PL spectra at different points in the micro-PL map

Moreover, an identical shape of the PL spectrum is found for both kind of samples (Fig. 2d) irrespective of the slight peak energy difference, indicating that the shift of the PL peak energy in the micro-PL maps comes from a local strain at a micrometer or sub-micrometer scale. The room temperature PL broadening, which comes from the homogeneous contribution, is ∼ 75 meV for both kind of samples.

Macro-PL (in blue) and transmittance (in red) spectra, acquired in the same spot of the sample, at 10 K are presented for $CsPbBr_3$ and $CsPbCl_3$ in Fig. 3a,b. The PL spectra show one main dominant peak at 2.33 eV and 2.97 eV for $CsPbBr_3$ and $CsPbCl_3$, respectively. Lower intensity contributions are also observed in both spectra: one at 2.32 eV for $CsPbBr_3$ and two at 3.0 eV and 3.03 eV for $CsPbCl_3$. The PL line broadening at 10 K for the main peak

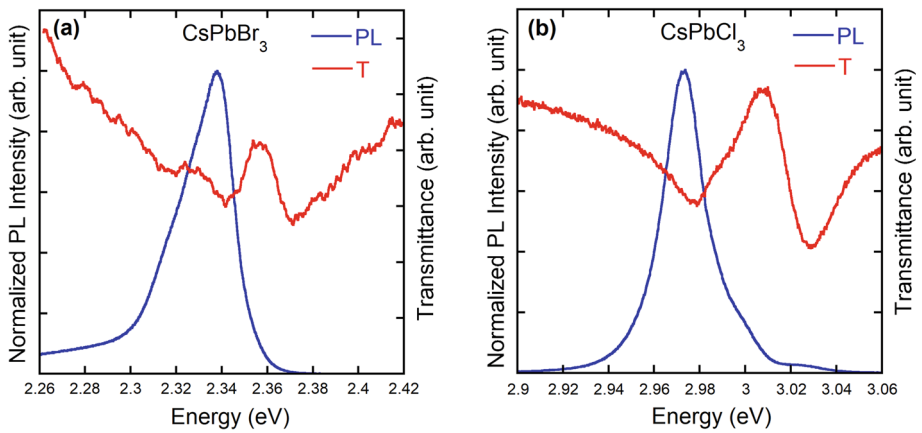

Fig. 3 Photoluminescence (PL) and transmittance (T) spectra at 10 K of a (**a**) $CsPbBr_3$ and a (**b**) $CsPbCl_3$ film deposited on glass

is ≤ 20 meV. This value is comparable with the one found at the same temperature in micro-PL measurements, indicating that it comes from disorder on a sub-micrometer scale, which is below the micro-PL resolution.

Both for $CsPbBr_3$ and $CsPbCl_3$, the low energy transmittance resonance and the PL dominant emission agree with literature data of bulk crystals and thin films [6]. More controversial is the attribution of the higher energy resonance observed in the transmittance spectra. For $CsPbBr_3$, given the energy separation (~ 30 meV) between the two transmittance minima compatible with the exciton binding energy [27], it could suggest that the high energy resonance comes from the 2S state. However, this attribution is unlikely, given the same amplitude of the resonances in the transmittance spectra. For $CsPbCl_3$ the high energy transmittance minimum corresponds to a PL band around 3.03 eV. Given the morphology of the $CsPbCl_3$ (Fig. 1c), where a compact layer of nanocrystals combined with the presence of micrometer crystals is evident, and in consideration of the time resolved results (see Fig. 4), the presence of the high energy transmittance minimum could be related to the nanocrystalline network (NCN). Therefore, having $CsPbBr_3$ and $CsPbCl_3$ a similar morphology (Fig. 1a,c), we more likely consider that also in the case of $CsPbBr_3$ the higher energy transmittance resonance comes from the NCN.

Recombination dynamics

The PL evolution on a time window of 800 ps is shown in the streak camera images (Fig. 4a,b) for both $CsPbBr_3$ and $CsPbCl_3$ at 10K, along with the normalized PL decays (Log scale) extracted from the image at three different energies. The three energies correspond to: low energy side due to emission in the Urbach tail (2.29 eV), localized exciton emission (2.33 eV), and free exciton recombination at 2.35 eV for $CsPbBr_3$; for $CsPbCl_3$ localized exciton emission (2.97 eV), free exciton recombination (2.99 eV), and at 3.02 eV the weak emission which corresponds to the high energy resonance observed in the transmittance spectrum of Fig. 3b. Non exponential decays are commonly found in this class of materials [24] with evidence of an exciton localization at low temperature and the presence of a high energy tail due to free carrier recombination. Comparable PL decay time constants for $CsPbBr_3$ and $CsPbCl_3$ are found: $\tau_1 \sim 40$ ps and $\tau_2 \sim 400$ ps. However, it should be noted that the fast component (τ_1) dominates in $CsPbCl_3$. An increase of the lifetime is observed up to ~ 90 K in both samples followed by an overall decrease, less than one order of magnitude, up to room temperature.

The Arrhenius curves (Fig. 5) for both kind of samples turn out to be very similar and can be fitted by the formula:

$$y = \frac{1}{1 + 25e^{-\frac{Ea_1}{kT}} + 2.7 \cdot 10^5 e^{-\frac{Ea_2}{kT}}} \tag{1}$$

where E_{a_1} and E_{a_2} are the two activation energies, which values are reported in Table 1.

In particular, the activation energy (95 meV) of the main non radiative channel does not agree with the exciton binding energy and therefore exciton ionization cannot describe the PL decrease at high temperature. As a consequence, the PL quenching more likely originates from a reduced number of carriers and excitons that initially populate the radiative states [18]. Moreover, having measured the PL yield at room temperature, from the Arrhenius plot we estimate a $\sim 90\%$ PL yield at 10 K, as expected for this kind of materials.

Our results prove that the deposition technique based on RF magnetron sputtering allows for the realization of high quality compact thin films comparable to state of the art samples.

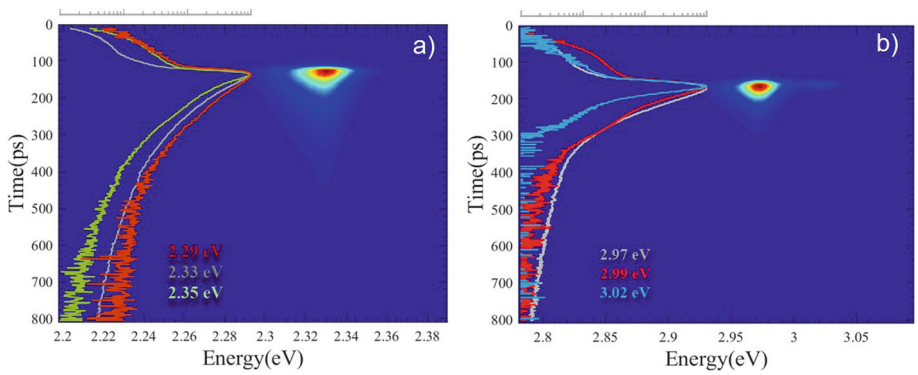

Fig. 4 Streak camera images at 10 K of a $CsPbBr_3$ (**a**) and a $CsPbCl_3$(**b**) film along with the normalized PL decays (Log scale) extracted from the image at three different energies

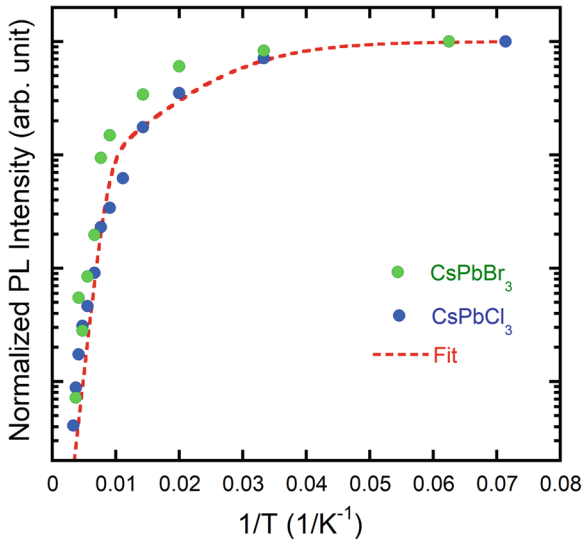

Fig. 5 Arrhenius curves for $CsPbBr_3$ (green) and $CsPbCl_3$ (blue) samples, obtained by plotting the PL intensity as a function of 1/T. The fitting curve (dashed red) is described by Eq. 1

Conclusions

Successful deposition of nanometric polycrystalline $CsPbBr_3$ and $CsPbCl_3$ films has been obtained by RF magnetron sputtering. This technique turns out to be promising in particular for $CsPbCl_3$ deposition, especially when limitations in realizing films by standard solution-based techniques are considered. Samples with film roughness below 20 nm for thickness ≥ 70 nm have been realized. The structural and optical properties of the as-deposited samples were investigated proving an overall quality, comparable to inorganic perovskites grown by solution-based techniques. Remarkable is the low value of PL broadening at low temperature, which is evidence of a submicrometric disorder. Indeed, through morphological and optical investigations, we observed the presence of a nanocrystalline network and fairly isolated sub-micrometer size crystals which can be ascribed to the sputtering deposition.

Having demonstrated the quality of several square centimeters samples realized by this technique, without the need of any post-growth treatment, we believe that RF magnetron sputtering could represent a very promising alternative to solution-based synthesis especially when multi-layer deposition is required for device realization.

Table 1 Values of the activation energies obtained by fitting the experimental data with Eq. 1

Activation energy	Value [meV]
E_{a_1}	10 ± 2
E_{a_2}	95 ± 5

Acknowledgements
Monica Bollani and Chiara Barri for SEM image of the $CsPbCl_3$ sample. Franco Bogani for discussions and critical reading of the manuscript.

Authors' contributions
NF wrote the paper. NF, AR, FB, GR, and AV performed the PL measurements. NC and SC grew the samples and performed the SEM investigations. PS performed the XRD investigations. AV assisted NF in writing the manuscript. The author(s) read and approved the final manuscript.

Funding
F.B. acknowledges funding from Fondazione Ente Cassa di Risparmio di Firenze within the project EPICO ("Eco-Perovskiti Inorganiche: Crescita e proprietà Optoelettroniche"; no. 2018.0950).

Availability of data and materials
The datasets used and/or analysed during the current study are available from the corresponding author on reasonable request.

Competing interests
The authors declare that they have no competing interests.

Author details
[1]Department of Physics and Astronomy, University of Florence, via G. Sansone 1, I-50019 Sesto Fiorentino, Italy. [2]European Laboratory for Non-Linear Spectroscopy - LENS, via Nello Carrara 1, I-50019 Sesto Fiorentino, Italy. [3]Industrial Engineering Department, University of Florence, via S. Marta 3, I-50139 Florence, Italy. [4]Interuniversity National Consortium for Material Science and Technology - INSTM, via Giusti 9, I-50121 Florence, Italy. [5]Department of Information Engineering, University of Brescia, via Branze 38, I-25123 Brescia, Italy. [6]Department of Civil, Environmental and Mechanical Engineering, University of Trento, via Mesiano 77, I-38123 Trento, Italy. [7]INFN-Firenze, via G. Sansone 1, I-50019 Sesto Fiorentino, Italy.

Received: 15 December 2020 Accepted: 19 May 2021
Published online: 02 June 2021

References

1. Kanemitsu, Y., Handa, T.: Photophysics of metal halide perovskites: From materials to devices. Jpn. J. Appl. Phys. **57**(9), 090101 (2018). https://doi.org/10.7567/jjap.57.090101

2. Song, J., Xu, L., Li, J., Xue, J., Dong, Y., Li, X., Zeng, H.: Monolayer and few-layer all-inorganic perovskites as a new family of two-dimensional semiconductors for printable optoelectronic devices. Adv. Mater. **28**(24), 4861–4869 (2016). https://doi.org/10.1002/adma.201600225
3. Zhang, J., Hodes, G., Jin, Z., Liu, S. F.: All-inorganic $CsPbX_3$ perovskite solar cells: progress and prospects. Angew. Chem. Int. Ed. **58**(44), 15596–15618 (2019). https://doi.org/10.1002/anie.201901081
4. Bruzzi, M., Talamonti, C., Calisi, N., Caporali, S., Vinattieri, A.: First proof-of-principle of inorganic perovskites clinical radiotherapy dosimeters. APL Mater. **7**(5), 051101 (2019). https://doi.org/10.1063/1.5083810
5. Protesescu, L., Yakunin, S., Bodnarchuk, M. I., Krieg, F., Caputo, R., Hendon, C. H., Yang, R. X., Walsh, A., Kovalenko, M. V.: Nanocrystals of cesium lead halide perovskites ($CsPbX_3$, X = Cl, Br, and I): novel optoelectronic materials showing bright emission with wide color gamut. Nano Lett. **15**(6), 3692–3696 (2015). https://doi.org/10.1021/nl5048779
6. Sebastian, M., Peters, J. A., Stoumpos, C. C., Im, J., Kostina, S. S., Liu, Z., Kanatzidis, M. G., Freeman, A. J., Wessels, B. W.: Excitonic emissions and above-band-gap luminescence in the single-crystal perovskite semiconductors $CsPbBr_3$ and $CsPbCl_3$. Phys. Rev. B. **92**(23) (2015). https://doi.org/10.1103/physrevb.92.235210
7. Kato, M., Fujiseki, T., Miyadera, T., Sugita, T., Fujimoto, S., Tamakoshi, M., Chikamatsu, M., Fujiwara, H.: Universal rules for visible-light absorption in hybrid perovskite materials. J. Appl. Phys. **121**(11), 115501 (2017). https://doi.org/10.1063/1.4978071
8. Bruzzi, M., Gabelloni, F., Calisi, N., Caporali, S., Vinattieri, A.: Defective states in micro-crystalline $CsPbBr_3$ and their role on photoconductivity. Nanomaterials. **9**(2), 177 (2019). https://doi.org/10.3390/nano9020177
9. Bruzzi, M., Falsini, N., Calisi, N., Vinattieri, A.: Electrically active defects in polycrystalline and single crystal metal halide perovskite. Energies. **13**(7), 1643 (2020). https://doi.org/10.3390/en13071643
10. Biccari, F., Falsini, N., Bruzzi, M., Gabelloni, F., Calisi, N., Vinattieri, A.: Defects in perovskites for solar cells and LEDs, Chapter 3. In: Ling, F. C., Zhou, S., Kuznetsov, A. (eds.) Defects in functional materials, pp. 49–91. World Scientific Publishing, Singapore, (2020)
11. Li, X., Cao, F., Yu, D., Chen, J., Sun, Z., Shen, Y., Zhu, Y., Wang, L., Wei, Y., Wu, Y., Zeng, H.: All inorganic halide perovskites nanosystem: synthesis, structural features, optical properties and optoelectronic applications. Small. **13**(9), 1603996 (2017). https://doi.org/10.1002/smll.201603996
12. Liang, K., Mitzi, D. B., Prikas, M. T.: Synthesis and characterization of organic-inorganic perovskite thin films prepared using a versatile two-step dipping technique. Chem. Mater. **10**(1), 403–411 (1998). https://doi.org/10.1021/cm970568f
13. Calisi, N., Caporali, S.: Investigation of open air stability of $CsPbBr_3$ thin-film growth on different substrates. Appl. Sci. **10**(21), 7775 (2020). https://doi.org/10.3390/app10217775
14. Calisi, N., Caporali, S., Milanesi, A., Innocenti, M., Salvietti, E., Bardi, U.: Composition-dependent degradation of hybrid and inorganic lead perovskites in ambient conditions. Top. Catal. **61**(9-11), 1201–1208 (2018). https://doi.org/10.1007/s11244-018-0922-5
15. Wang, R., Mujahid, M., Duan, Y., Wang, Z.-K., Xue, J., Yang, Y.: A review of perovskites solar cell stability. Adv. Funct. Mater. **29**(47), 1808843 (2019). https://doi.org/10.1002/adfm.201808843
16. Sim, K., Jun, T., Bang, J., Kamioka, H., Kim, J., Hiramatsu, H., Hosono, H.: Performance boosting strategy for perovskite light-emitting diodes. Appl. Phys. Rev. **6**(3), 031402 (2019). https://doi.org/10.1063/1.5098871
17. Borri, C., Calisi, N., Galvanetto, E., Falsini, N., Biccari, F., Vinattieri, A., Cucinotta, G., Caporali, S.: First proof-of-principle of inorganic lead halide perovskites deposition by magnetron-sputtering. Nanomaterials. **10**(1), 60 (2019). https://doi.org/10.3390/nano10010060
18. Falsini, N., Calisi, N., Roini, G., Ristori, A., Biccari, F., Scardi, P., Barri, C., Bollani, M., Caporali, S., Vinattieri, A.: Large-area nanocrystalline caesium lead chloride thin films: a focus on the exciton recombination dynamics. Nanomaterials. **11**(2), 434 (2021). https://doi.org/10.3390/nano11020434
19. Gulbiński, W.: Deposition of Thin Films by Sputtering. In: Pauleau, Y. (ed.) Chemical physics of thin film deposition processes for micro- and nano-technologies. Springer, Netherlands, (2002)
20. Greene, J. E.: Review article: tracing the recorded history of thin-film sputter deposition: from the 1800s to 2017. J. Vac. Sci. Technol. A Vac. Surf. Films. **35**(5), 05–204 (2017). https://doi.org/10.1116/1.4998940
21. Gudmundsson, J. T.: Physics and technology of magnetron sputtering discharges. Plasma Sources Sci. Technol. **29**(11), 113001 (2020). https://doi.org/10.1088/1361-6595/abb7bd
22. Bonomi, S., Marongiu, D., Sestu, N., Saba, M., Patrini, M., Bongiovanni, G., Malavasi, L.: Novel physical vapor deposition approach to hybrid perovskites: growth of $MAPbI_3$ thin films by RF-magnetron sputtering. Sci. Rep. **8**(1) (2018). https://doi.org/10.1038/s41598-018-33760-w
23. Jana, A., Mittal, M., Singla, A., Sapra, S.: Solvent-free, mechanochemical syntheses of bulk trihalide perovskites and their nanoparticles. Chem. Commun. **53**(21), 3046–3049 (2017). https://doi.org/10.1039/c7cc00666g
24. Gabelloni, F., Biccari, F., Falsini, N., Calisi, N., Caporali, S., Vinattieri, A.: Long-living nonlinear behavior in $CsPbBr_3$ carrier recombination dynamics. Nanophotonics. **8**(9), 1447–1455 (2019). https://doi.org/10.1515/nanoph-2019-0013
25. Stoumpos, C. C., Malliakas, C. D., Peters, J. A., Liu, Z., Sebastian, M., Im, J., Chasapis, T. C., Wibowo, A. C., Chung, D. Y., Freeman, A. J., Wessels, B. W., Kanatzidis, M. G.: Crystal growth of the perovskite semiconductor $CsPbBr_3$: a new material for high-energy radiation detection. Cryst. Growth Des. **13**(7), 2722–2727 (2013). https://doi.org/10.1021/cg400645t
26. Iwanaga, M.: Photoacoustic detection of phase transitions at low temperatures in $CsPbCl_3$ crystals. Phase Transit. **78**(5), 377–385 (2005). https://doi.org/10.1080/01411590500114732
27. Li, J., Yuan, X., Jing, P., Li, J., Wei, M., Hua, J., Zhao, J., Tian, L.: Temperature-dependent photoluminescence of inorganic perovskite nanocrystal films. RSC Adv. **6**(82), 78311–78316 (2016). https://doi.org/10.1039/c6ra17008k

Publisher's Note